g modes of neutron stars with hadron-to-quark crossover transitions

Constantinos Constantinou,[1,2,*] Sophia Han (韩君),[3,4,†] Prashanth Jaikumar,[5,‡] and Madappa Prakash[6,§]

[1]*INFN-TIFPA, Trento Institute of Fundamental Physics and Applications, Povo 38123 TN, Italy*
[2]*European Centre for Theoretical Studies in Nuclear Physics and Related Areas, Villazzano 38123 TN, Italy*
[3]*Institute for Nuclear Theory, University of Washington, Seattle, Washington 98195, USA*
[4]*Department of Physics, University of California, Berkeley, California 94720, USA*
[5]*Department of Physics and Astronomy, California State University Long Beach, Long Beach, California 90840, USA*
[6]*Department of Physics and Astronomy, Ohio University, Athens, Ohio 45701, USA*

(Received 28 September 2021; accepted 14 November 2021; published 22 December 2021)

We perform the first study of the principal core g-mode oscillation in hybrid stars containing quark matter, utilizing a crossover model for the hadron-to-quark transition inspired by lattice QCD. The ensuing results are compared with our recent findings of g-mode frequencies in hybrid stars with a first-order phase transition using Gibbs constructions. We find that models using Gibbs construction yield g-mode amplitudes and the associated gravitational energy radiated that dominate over those of the chosen crossover model owing to the distinct behaviors of the equilibrium and adiabatic sound speeds in the various models. Based on our results, we conclude that were g modes to be detected in upgraded LIGO and Virgo detectors it would indicate a first-order phase transition akin to a Gibbs construction.

DOI: 10.1103/PhysRevD.104.123032

I. INTRODUCTION

Dense matter inside neutron stars (NSs) could contain unbound quarks that retain some vestige of the forces described by the fundamental theory of the strong interaction, quantum chromodynamics (QCD). Lacking exact methods for its solution, numerous models have been constructed to investigate the hadron-to-quark transition in the region of high baryon density and zero temperature. On the other hand, the phase diagram of QCD at low density (zero or small baryon chemical potential) and high temperature is amenable to precision numerical studies which clearly point to a crossover with no clear phase boundary between the hadron resonance gas and the quark-gluon plasma [1].

Recently, Kapusta and Welle [2] (KW hereafter) have proposed a crossover model for the hadron-to-quark transition in NSs to mimic the crossover feature of finite temperature lattice studies. The key trait of this model is an analytic mixing or switching function that accounts for the partial pressure of each component as a function of a single parameter—the baryon chemical potential. They found that NSs as massive as $\sim 2.2\ M_\odot$ could be supported by their crossover equation of state (EOS). As hadrons/nucleons and quarks both appear explicitly as separate degrees of freedom in the KW description, it is straightforward to keep track of their individual contributions to the total pressure. KW report that, within their model, between 1–10% of the total pressure could be contributed by quark matter in the core. In treatments in which hadron and quark interactions are intermingled, the individual contributions from hadrons and quarks to the total pressure may not be possible to disentangle. Given that EOSs with first-order phase transitions treated using the Maxwell construction face some challenges in obtaining the stable $\sim 2\ M_\odot$ NSs that have been observed, it is worthwhile to investigate alternatives such as the crossover model for hybrid stars.

Our objective in this paper is twofold: first, we extend the pure neutron matter (PNM) model of KW [2] to include β equilibrium, as well as a crust for the hybrid star. We also include vector interactions among quarks. These modifications enable a direct comparison to other approaches in the literature [3]. Second, we investigate g-mode oscillations, a potentially observable signature of the hadron-to-quark transition. A g mode is a specific fluid oscillation where a parcel of fluid is displaced against the background of a stratified environment inside a neutron star. While pressure equilibrium is rapidly restored via sound waves, chemical equilibrium can take longer, causing buoyancy forces to oppose the displacement. Since cold NSs are not convective, the opposing force sets up stable oscillations, with a typical frequency, called the (local) Brunt-Väisälä frequency. The kind of core g modes we study here were

*cconstantinou@ectstar.eu
†sjhan@uw.edu
‡prashanth.jaikumar@csulb.edu
§prakash@ohio.edu

introduced in [4–7] and in a recent work, which we shall refer to as paper I [8], we showed that the g-mode frequency rises steeply with the onset of quarks due to a rapid change in the equilibrium sound speed (see also Ref. [9]). Since g-mode oscillations couple to tidal forces, they may be excited during the merger of two NSs and provide information on the interior composition, specifically quarks here. In paper I, we chose a Gibbs construction for the mixed phase, which yields NS properties that are more compatible with astrophysical constraints than a Maxwell construction.[1] In this work, we present the systematics of the g-mode frequency for hybrid stars in a crossover scenario, adopting the generalized KW model as a representative of this class. It is worth noting that Maxwell-constructed first-order phase transitions cannot generate g modes in the transition region, because the equilibrium and adiabatic sound speeds both become zero (due to frozen pressure and composition over the phase coexistence region) there.

In the first phase of this work, we will restrict ourselves to zero temperature without the effects of superfluidity in both nucleons and quarks. To the best of our knowledge, this is the first study of g mode for hybrid stars in a crossover model. References to earlier work in which hadronic EOSs with and without superfluidity were used to investigate g-mode frequencies can be found in paper I (see Refs. [21–35] therein).

Models akin to the crossover model of KW, but with some differences, have been considered earlier in the literature. Examples include the smooth crossover model of Ref. [10], interpolated EOSs considered in Refs. [11–14], and quarkyonic models of Refs. [15–18], et cetera. In the chiral model of Refs. [19–21], a scalar field Φ, acting as an order parameter, is responsible for the deconfinement phase transition which can be first order or crossover depending upon temperature and baryon chemical potential. Depending on the specific EOS models used in the hadronic and quark phases, chemical potential and pressure equilibrium between the two phases—of either the Maxwell or the Gibbs sort—may not be realized [11]. In such cases, several interpolation procedures have been adopted to connect the two phases on the premise that at high supranuclear densities, a purely hadronic phase is untenable.

In quarkyonic models with a momentum shell structure [15,16], quarks emerge at relatively low (but still suprasaturation) densities but remain bound by strong interactions below the Fermi surface: while hadrons and quarks are separated in momentum space, they coexist in configuration space. A key parameter that enters the calculation of the g mode is the squared adiabatic speed of sound $c_{\rm ad}^2 = (\partial P/\partial \varepsilon)|_{y_i,\beta}$, where P and ε are the total pressure and energy density, respectively, and $y_{i,\beta}$ refer to the partial fractions of each component in beta equilibrium.[2] We find that in the quarkyonic "shell" models of Refs. [15,16], $c_{\rm ad}^2$ becomes discontinuous with respect to density at the shell boundary. To address g modes in this specific category of quarkyonic shell models, and to extend the study of NS oscillations to span the various ways in which quarks can affect the dense matter EOS and the properties of NSs, such discontinuities must be smoothed. As such a task is outside the scope of the present work, we do not consider these quarkyonic models in this paper.

The organization of this paper is as follows. In Sec. II, we describe the EOSs for pure hadronic matter, pure quark matter and leptons used in the construction of the KW crossover model of Ref. [2] by extending it to include β equilibrium and interactions between quarks. The rationale for our parameter choices and the basic features of this model are also highlighted here for orientation. Section III reviews the thermodynamics of a multicomponent system as pertinent to the KW description of crossover matter generalized here to describe neutron-star matter (NSM). In Sec. IV, the KW model formulation of crossover matter is described followed by the procedure to render the unconstrained system[3] in β equilibrium. This section also contains a comparison of the extended KW model with those of selected quarkyonic shell models. In Sec. V, the calculation of the equilibrium and adiabatic sound speeds in the crossover and Gibbs approaches are outlined. In Sec. VI, we present results for the chosen EOSs and their associated NS structural properties as well as the two speeds of sound in the crossover model, and discuss emergent differences from other models that include a phase transition. This section also contains results for the sound speed difference, the Brunt-Väisälä frequency, and the g-mode frequency in hybrid stars along with their interpretation. Our conclusions and outlook are in Sec. VII.

II. EQUATION OF STATE

In the KW description of the crossover transition, EOSs in the pure hadronic and quark phases are combined using a mixing or switch function that depends on the baryon chemical potential (to be described below). We therefore begin by discussing EOS models that we use in each of these two sectors. As we extend the KW model to include leptons, the EOS in the leptonic sector is also provided. These EOSs are first set forth without reference to baryon number conservation, charge neutrality, as well as chemical

[1] See Table VII in Ref. [3] for a comprehensive comparison of Gibbs, Maxwell and certain crossover models.

[2] $c_{\rm ad}^2$ is different from the squared equilibrium speed of sound $c_{\rm eq}^2 = dP/d\varepsilon$ commonly defined as c_s^2 in the literature for static EOS models.

[3] The unconstrained system here refers to matter in which baryon number conservation, charge neutrality and β equilibrium are not imposed.

equilibrium (i.e., unconstrained), which are imposed at the appropriate junctures.

A. Pure hadronic matter

To describe nucleons, we use the Zhao-Lattimer (ZL) [16] parametrization of the EOS of neutron-star matter. With reasonable adjustments of its parameters, this EOS can be made consistent with laboratory data at nuclear saturation density $n_{\rm sat} \simeq 0.16$ fm^{-3} as well as recent chiral effective field theory calculations of Refs. [22,23] in which error quantifications up to $\sim 2.0 n_{\rm sat}$ were made. The high-density behavior can be controlled by varying the slope of the symmetry energy parameter, L, at $n_{\rm sat}$ within the range established from analyses of nuclear and observational data, see, e.g., Ref. [24], and a power-law index. Consistency with astrophysical data on known masses and radii of NSs is also attainable with this EOS.

To begin with, no constraints are placed on the multi-particle system and therefore the independent variables are the baryon density $n_{\rm B}$ and the individual particle fractions y_n, y_p. The total energy density of nucleons with a common mass $m_H = 939.5$ MeV is described by the ZL functional

$$\begin{aligned}\varepsilon_H = &\frac{1}{8\pi^2\hbar^3}\sum_{h=n,p}\left\{k_{Fh}(k_{Fh}^2+m_H^2)^{1/2}(2k_{Fh}^2+m_H^2)\right.\\ &\left.-m_H^4\ln\left[\frac{k_{Fh}+(k_{Fh}^2+m_H^2)^{1/2}}{m_H}\right]\right\}\\ &+4n_{\rm B}^2 y_n y_p\left\{\frac{a_0}{n_{\rm sat}}+\frac{b_0}{n_{\rm sat}^{\gamma}}[n_{\rm B}(y_n+y_p)]^{\gamma-1}\right\}\\ &+n_{\rm B}^2(y_n-y_p)^2\left\{\frac{a_1}{n_{\rm sat}}+\frac{b_1}{n_{\rm sat}^{\gamma_1}}[n_{\rm B}(y_n+y_p)]^{\gamma_1-1}\right\}. \end{aligned} \tag{1}$$

The Fermi momentum of nucleon species h[4] is given by $k_{Fh} = (3\pi^2\hbar^3 n_{\rm B} y_h)^{1/3}$. The constants a_0, b_0 and γ refer to isospin symmetric matter, whereas a_1, b_1 and γ_1 refer to that of isospin asymmetric matter. The chosen values of these constants are listed in a later section.

The corresponding chemical potentials are

$$\begin{aligned}\mu_n = &(k_{Fn}^2+m_H^2)^{1/2}+4n_{\rm B}y_p\left\{\frac{a_0}{n_{\rm sat}}+\frac{b_0}{n_{\rm sat}^{\gamma}}[n_{\rm B}(y_n+y_p)]^{\gamma-1}\right\}\\ &+4n_{\rm B}^2 y_p y_n\frac{b_0}{n_{\rm sat}^{\gamma}}(\gamma-1)[n_{\rm B}(y_n+y_p)]^{\gamma-2}\\ &+2n_{\rm B}(y_n-y_p)\left\{\frac{a_1}{n_{\rm sat}}+\frac{b_1}{n_{\rm sat}^{\gamma_1}}[n_{\rm B}(y_n+y_p)]^{\gamma_1-1}\right\}\\ &+n_{\rm B}^2(y_n-y_p)^2\frac{b_1}{n_{\rm sat}^{\gamma_1}}(\gamma_1-1)[n_{\rm B}(y_n+y_p)]^{\gamma_1-2}, \end{aligned} \tag{2}$$

$$\begin{aligned}\mu_p = &(k_{Fp}^2+m_H^2)^{1/2}+4n_{\rm B}y_n\left\{\frac{a_0}{n_{\rm sat}}+\frac{b_0}{n_{\rm sat}^{\gamma}}[n_{\rm B}(y_n+y_p)]^{\gamma-1}\right\}\\ &+4n_{\rm B}^2 y_p y_n\frac{b_0}{n_{\rm sat}^{\gamma}}(\gamma-1)[n_{\rm B}(y_n+y_p)]^{\gamma-2}\\ &-2n_{\rm B}(y_n-y_p)\left\{\frac{a_1}{n_{\rm sat}}+\frac{b_1}{n_{\rm sat}^{\gamma_1}}[n_{\rm B}(y_n+y_p)]^{\gamma_1-1}\right\}\\ &+n_{\rm B}^2(y_n-y_p)^2\frac{b_1}{n_{\rm sat}^{\gamma_1}}(\gamma_1-1)[n_{\rm B}(y_n+y_p)]^{\gamma_1-2}. \end{aligned} \tag{3}$$

Note the opposite y_h and signs in the second and fourth terms of μ_n and μ_p, respectively.

The pressure is obtained from the thermodynamic identity

$$P_H = n_{\rm B}\sum_{h=n,p}\mu_h y_h - \varepsilon_H \tag{4}$$

and the equilibrium speed of sound from

$$\left(\frac{c_{\rm eq}}{c}\right)^2 = \frac{dP_H}{d\varepsilon_H}. \tag{5}$$

The adiabatic speed of sound is obtained by taking partial derivatives of the pressure and the total energy density with respect to baryon density while keeping all particle fractions fixed

$$\left(\frac{c_{\rm ad}}{c}\right)^2 = \left.\frac{\partial P_H}{\partial n_{\rm B}}\right|_{y_h}\left(\left.\frac{\partial \varepsilon_H}{\partial n_{\rm B}}\right|_{y_h}\right)^{-1}. \tag{6}$$

This is made particularly convenient by the choice of starting with a completely unconstrained system.

B. Pure quark matter

For the calculation of the quark EOS, we use the vMIT bag model [25,26]. The Lagrangian density of this model is

$$\mathcal{L} = \sum_{q=u,d,s}[\bar{\psi}_q(i\partial\!\!\!/ - m_q - B)\psi_q + \mathcal{L}_{\rm vec}]\Theta, \tag{7}$$

where $\mathcal{L}_{\rm vec}$ describes repulsive interactions between quarks of mass m_q confined within a bag as denoted by the Θ function:

$$\mathcal{L}_{\rm vec} = -G_v\sum_q \bar{\psi}\gamma_\mu V^\mu\psi + (m_V^2/2)V_\mu V^\mu. \tag{8}$$

B is a constant which reflects the cost of confining the quarks inside the bag, and the m_q are the current quark masses. Perturbative contributions [27,28] are not included in vMIT because these become relevant at densities well above those achievable in the cores of the most massive neutron stars.

[4]While the symbols "H" and "h" connote hadrons, they actually refer to nucleons in the context of this paper.

The state functions, energy density, chemical potential and pressure, corresponding to the above Lagrangian (*before* any constraints of baryon number conservation, charge neutrality, and chemical equilibrium are applied) for matter containing u, d and s quarks are

$$\varepsilon_Q = \sum_{q=u,d,s} \varepsilon_q + \frac{1}{2} a\hbar[n_{\rm B}(y_u + y_d + y_s)]^2 + \frac{B}{\hbar^3}, \quad (9)$$

$$\varepsilon_q = \frac{3}{8\pi^2\hbar^3}\left\{ k_{Fq}(k_{Fq}^2 + m_q^2)^{1/2}(2k_{Fq}^2 + m_q^2) - m_q^4 \ln\left[\frac{k_{Fq} + (k_{Fq}^2 + m_q^2)^{1/2}}{m_q}\right]\right\}, \quad (10)$$

$$\mu_q = (k_{Fq}^2 + m_q^2)^{1/2} + a\hbar n_{\rm B}(y_u + y_d + y_s), \quad (11)$$

$$P_Q = n_{\rm B} \sum_{q=u,d,s} \mu_q y_q - \varepsilon_Q, \quad (12)$$

where $a \equiv (G_v/m_V)^2$ and $k_{Fq} = (\pi^2\hbar^3 n_{\rm B} y_q)^{1/3}$. The value of the vector interaction parameter a is varied in the range (0.1–0.3) fm^{-2} to obtain different stiffness in the quark sector.

C. Leptons

Owing to the smallness of the electromagnetic fine structure constant $\alpha \simeq 1/137$, leptons are treated as noninteracting, relativistic particles for which

$$\varepsilon_L = \frac{1}{8\pi^2\hbar^3}\sum_l \left\{ k_{Fl}(k_{Fl}^2 + m_l^2)^{1/2}(2k_{Fl}^2 + m_l^2) - m_l^4 \ln\left[\frac{k_{Fl} + (k_{Fl}^2 + m_l^2)^{1/2}}{m_l}\right]\right\}, \quad (13)$$

$$\mu_l = (k_{Fl}^2 + m_l^2)^{1/2}, \quad (14)$$

$$P_L = n_{\rm B}\sum_l y_l\mu_l - \varepsilon_L, \quad (15)$$

$$k_{Fl} = (3\pi^2\hbar^3 n_{\rm B} y_l)^{1/3}; \qquad l = e, \mu. \quad (16)$$

At low baryon densities only electrons are present in the system, with muons appearing at a density $n_{\rm B}$ such that $\mu_e - m_\mu = 0$. Depending on the parametrization choice, this condition also gives the density at which muons vanish.

III. THERMODYNAMICS OF MULTICOMPONENT SYSTEMS

The original formulation of the KW approach deals with one nucleon, the neutron, and three massless quarks (the latter are, operationally, a single species with multiplicity 3). Before the KW approach can be applied to more realistic neutron-star matter with the EOSs of the previous section, it must be generalized to include several particle species. To that end, we begin with a brief review of multicomponent thermodynamics to introduce the fundamental result from which the aforementioned generalization will be performed in the next section. The relations laid out below are particularly helpful in highlighting the role of the (baryon chemical potential dependent) switch function S, which is instrumental in realizing a crossover transition.

The number density of a single-component system in the grand-canonical ensemble is given by the total derivative of the pressure with respect to the chemical potential,

$$n = \frac{dP}{d\mu}. \quad (17)$$

The equivalent expression for a multicomponent system is obtained from the grand potential

$$\Phi(T, V, \mu_i) = U - TS - \sum_i N_i\mu_i \quad (18)$$

or, in units of energy density,

$$\phi = \varepsilon - Ts - \sum_i n_i\mu_i. \quad (19)$$

The differential of ϕ is

$$d\phi = d\varepsilon - sdT - \sum_i n_i d\mu_i, \quad (20)$$

which implies that the number density of particle species i is given by

$$n_i = -\left.\frac{\partial\phi}{\partial\mu_i}\right|_{T,\mu_j}. \quad (21)$$

The thermodynamic identity

$$\varepsilon = Ts - P + \sum_i n_i\mu_i \quad (22)$$

means that $P = -\phi$ and therefore

$$n_i = \left.\frac{\partial P}{\partial\mu_i}\right|_{\mu_j}, \quad (23)$$

where the temperature T has been suppressed as, in what follows, only cold matter is considered.

Equation (23) is central to the subsequent discussion where we show the manner in which the individual number densities of the various nucleonic and quark species are modified by the switch function S of the KW machinery.

IV. UNCONSTRAINED AND BETA-EQUILIBRATED CROSSOVER MATTER

In this section, we start with the crossover EOS where baryon number conservation, charge neutrality, and weak interaction equilibrium are not imposed, i.e., "unconstrained" matter. Working with unconstrained quantities enables us to calculate the various partial derivatives required in the determination of the squared adiabatic speed of sound $c_{\rm ad}^2$ (see Sec. V) prior to the imposition of the conditions mentioned above.

In the KW description of crossover matter, the pressure is given by

$$P_B = (1-S)P_H + SP_Q, \tag{24}$$

where P_H and P_Q are the hadron and quark pure-phase pressures, respectively, and the switch function

$$S = \exp\left[-\left(\frac{\mu_0}{\mu}\right)^4\right] \tag{25}$$

gives the fraction of quark matter to the total baryonic matter in the crossover setting, with μ being the average hadronic chemical potential

$$\mu = \frac{n_n\mu_n + n_p\mu_p}{n_n + n_p}, \tag{26}$$

and μ_0 a typical energy scale for the crossover. This choice for μ will be justified in the next section.

Applying Eq. (23) to hadrons leads to

$$\begin{aligned} n_h^* &= (1-S)\frac{\partial P_H}{\partial \mu_h} + S\frac{\partial P_Q}{\partial \mu_h} + (P_Q - P_H)\frac{\partial S}{\partial \mu_h}, \\ &= (1-S)n_h + 0 + (P_Q - P_H)\frac{4\mu_0^4 S}{\mu^5}\frac{\partial \mu}{\partial \mu_h}, \\ &= (1-S)n_h + (P_Q - P_H)\frac{4\mu_0^4 S}{\mu^5}\frac{n_h}{n_n + n_p}, \\ &= n_h\left[1 - S\left(1 - \frac{4\mu_0^4}{\mu^5}\frac{P_Q - P_H}{n_n + n_p}\right)\right], \end{aligned} \tag{27}$$

where $n_i^* = n_{\rm B} y_i^*$ refers to a crossover-matter density and $n_i = n_{\rm B} y_i$ to a pure-phase density. Thus, in the present context, the starred fractions are the physical quantities, whereas the unstarred ones are merely bookkeeping devices. For leptons this distinction is irrelevant.

For quarks, one obtains

$$\begin{aligned} n_q^* &= (1-S)\frac{\partial P_H}{\partial \mu_q} + S\frac{\partial P_Q}{\partial \mu_q} + (P_Q - P_H)\frac{\partial S}{\partial \mu_q}, \\ &= 0 + Sn_q + 0 = Sn_q. \end{aligned} \tag{28}$$

Finally, the energy density ε is obtained from Eq. (22) using Eq. (24) for the pressure, Eqs. (27)–(28) for the number densities of hadrons and quarks, respectively, and the pure-phase chemical potentials defined in Sec. II.

A. Beta equilibrium

We turn now to the discussion of neutron-star matter that consists of nucleons, leptons and quarks. Initially, the system is entirely unconstrained with $n_{\rm B}$ and y_i $(i = n, p, u, d, s, e, \mu)$ as the free variables. Then, strong equilibrium

$$\mu_n = 2\mu_d + \mu_u, \qquad \mu_p = 2\mu_u + \mu_d, \tag{29}$$

and weak equilibrium

$$\mu_n = \mu_p + \mu_e, \qquad \mu_e = \mu_\mu, \qquad \mu_d = \mu_s, \tag{30}$$

are enforced, as well as charge neutrality

$$n_p^* + (2n_u^* - n_d^* - n_s^*)/3 - (n_e + n_\mu) = 0 \tag{31}$$

and baryon number conservation

$$n_n^* + n_p^* + (n_u^* + n_d^* + n_s^*)/3 - n_{\rm B} = 0. \tag{32}$$

These conditions eliminate the particle fractions in favor of the total baryon density:

$$y_i \to y_{i,\beta}(n_{\rm B}), \qquad i = n, p, u, d, s, e, \mu. \tag{33}$$

B. Comparison of KW with McLerran-Reddy and Zhao-Lattimer EOSs

In this subsection, we briefly discuss interesting similarities and differences between the crossover model of KW [2] and recently proposed quarkyonic "shell" models of McLerran-Reddy (MR) [15] and Zhao-Lattimer (ZL) [16], and explain the reason why the latter is not suitable for g-mode calculations in its present form. The baryon number densities in the quarkyonic matter descriptions of MR [15] and ZL [16] are

$$n_h^* = \frac{k_{Fh}^3 - k_{0h}^3}{3\pi^2\hbar^3} = \frac{k_{Fh}^3}{3\pi^2\hbar^3}\left(1 - \frac{k_{0h}^3}{k_{Fh}^3}\right) = n_h\left(1 - \frac{k_{0h}^3}{k_{Fh}^3}\right), \tag{34}$$

where k_{0h} are the minimum momenta of hadrons or nucleons in quarkyonic matter, which depend on the corresponding Fermi momenta k_{Fh} and thus the baryon number density. The precise way in which $k_{Fh} - k_{0h}$ depends on a chosen momentum scale Λ and a common transition density n_t is detailed in Eq. (17) of Ref. [16].

Comparing the above expression to Eq. (27) from the previous section, it becomes clear that the presence of the hadron shell in the MR and ZL approaches forces hadrons to higher-momentum states much like S does in the KW scheme:

$$S\left(1-\frac{4\mu_0^4}{\mu^5}\frac{P_Q-P_H}{n_n+n_p}\right)\hat{=}\frac{k_{0h}^3}{k_{Fh}^3}. \tag{35}$$

This means that any particle species participating in $S(\mu)$ (that is, a species i for which $\partial\mu/\partial\mu_i \neq 0$) will invariably inherit a shell-like term in its crossover-matter number density. In quarkyonic matter realizations, such a term is desirable for baryons but not for quarks and therefore μ must be a function of baryonic chemical potentials only.

Note that in the case of KW, the quark densities in crossover-matter n_q^* are the product of the corresponding pure-phase densities and the quark-to-baryon fraction S which is an *a priori* assumption. On the other hand, for both MR and ZL models, the densities and fractions of baryons and quarks in the quarkyonic phase are determined by the solution of the equilibrium equations.

Here, we should point out that in the MR and ZL implementations of the quarkyonic matter scenario, the nucleonic Fermi momenta are weakly dependent on baryon density when the latter exceeds the transition density, n_t; that is,

$$|k_{\infty,i}-k_{Fi,\beta}|/k_{\infty,i} \ll 1 \quad \text{for all } n_{\rm B} > n_t, \tag{36}$$

where $k_{\infty,i} \equiv k_{Fi,\beta}(n_{\rm B}\to\infty)$. On the other hand, the nucleonic chemical potentials and, by extension, the pressure change very rapidly with k_{Fi} for $n_{\rm B} > n_t$ due to the presence of denominators $\propto (1-K_i)$ [see Eqs. (19)–(20) in [16]] in their kinetic parts, where

$$K_i^{\rm MR} = \left(\frac{k_{0i}}{k_{Fi}}\right)^2\left(1+\frac{2\Lambda^3}{k_{Fi}^3}\right), \tag{37}$$

$$K_i^{\rm ZL} = \left(\frac{k_{0i}}{k_{Fi}}\right)^2\left(1+\frac{\Lambda^2}{k_{Fi}^2}\right). \tag{38}$$

These terms remain close to zero [i.e., $(1-K_i)^{-1}\to\infty$], in equilibrium matter as a result of the aforementioned behavior of the nucleonic Fermi momenta, throughout the quarkyonic regime. These two features of MR and ZL are responsible for divergent pressure derivatives with respect to k_{Fi} which, in turn, lead to superluminal adiabatic sound speeds. Thus MR and ZL, in their current formulations, are unsuitable for our purposes and we do not apply them in g-mode calculations for crossover matter.

V. SOUND SPEEDS

In this section, we describe how calculations of the squared adiabatic and equilibrium sound speeds, $c_{\rm ad}^2$ and $c_{\rm eq}^2$, required in the calculation of g-mode frequencies, are performed. As one of our objectives is to provide contrasts between g-mode frequencies in crossover matter and the case of a first-order transition treated via the Gibbs construction, both cases are considered below.

A. Sound speeds in crossover matter

Within the KW framework, the total pressure and energy density in the crossover region are

$$P = P_B + P_e + P_\mu, \tag{39}$$

$$\varepsilon = \varepsilon_B + \varepsilon_e + \varepsilon_\mu, \tag{40}$$

$$\varepsilon_B = -P_B + \sum_{i=n,p,u,d,s} n_i^*\mu_i. \tag{41}$$

Using these, the adiabatic speed of sound is obtained by first calculating the expression

$$c_{\rm ad}^2(n_{\rm B},y_i) = \left.\frac{\partial P}{\partial n_{\rm B}}\right|_{y_i}\left(\left.\frac{\partial\varepsilon}{\partial n_{\rm B}}\right|_{y_i}\right)^{-1} \tag{42}$$

and then evaluating it in β equilibrium

$$c_{ad,\beta}^2(n_{\rm B}) = c_{\rm ad}^2[n_{\rm B},y_{i,\beta}(n_{\rm B})]. \tag{43}$$

The equilibrium sound speed is given by the total derivatives of the pressure and the energy density with respect to the baryon density after the enforcement of β equilibrium,

$$c_{\rm eq}^2 = \frac{dP_\beta}{dn_{\rm B}}\left(\frac{d\varepsilon_\beta}{dn_{\rm B}}\right)^{-1}. \tag{44}$$

B. Sound speeds with Gibbs construction

As in the crossover matter case, all thermodynamic quantities are expressed in terms of functions of the total baryon density $n_{\rm B}$, and the individual particle fractions y_n, y_p, y_e, y_μ, y_u, y_d, y_s which are, at this point, independent variables. That is,

$$\varepsilon_H = \varepsilon_H(n_{\rm B},y_n,y_p), \qquad P_H = P_H(n_{\rm B},y_n,y_p),$$
$$\mu_h = \mu_h(n_{\rm B},y_n,y_p), \tag{45}$$

$$\varepsilon_Q = \varepsilon_Q(n_{\rm B},y_u,y_d,y_s), \qquad P_Q = P_Q(n_{\rm B},y_u,y_d,y_s),$$
$$\mu_q = \mu_q(n_{\rm B},y_q), \tag{46}$$

$$\varepsilon_L = \varepsilon_L(n_{\rm B},y_e,y_\mu), \qquad P_L = P_L(n_{\rm B},y_e,y_\mu),$$
$$\mu_l = \mu_l(n_{\rm B},y_l). \tag{47}$$

The conditions for weak equilibrium, charge neutrality and baryon number conservation are applied afterwards. These introduce another independent variable, χ, which is the volume fraction of quarks in the mixed phase of Gibbs construction:

$$P_H = P_Q, \qquad \mu_n = 2\mu_d+\mu_u, \qquad \mu_p = 2\mu_u+\mu_d, \tag{48}$$

$$\mu_n = \mu_p + \mu_e, \qquad \mu_e = \mu_\mu, \qquad \mu_d = \mu_s, \tag{49}$$

$$3(1-\chi)y_p + \chi(2y_u - y_d - y_s) - 3(y_e + y_\mu) = 0, \tag{50}$$

$$3(1-\chi)(y_n + y_p) + \chi(y_u + y_d + y_s) - 3 = 0. \tag{51}$$

Solving these equations eliminates the y_i and χ in favor of $n_{\rm B}$. Thus the state variables become functions of only $n_{\rm B}$ according to the rule

$$Q(n_{\rm B}, y_i, y_j, \ldots) \to Q[n_{\rm B}, y_i(n_{\rm B}), y_j(n_{\rm B}), \ldots] = Q(n_{\rm B}).$$

Then, the thermodynamics of the mixed $(^*)$ phase are

$$\varepsilon^* = (1-\chi)\varepsilon_H + \chi\varepsilon_Q + \varepsilon_L, \tag{52}$$

$$\begin{aligned} P^* &= P_H + P_L = P_Q + P_L, \\ &= (1-\chi)P_H + \chi P_Q + P_L, \end{aligned} \tag{53}$$

$$\mu_h^* = \mu_h, \qquad \mu_q^* = \mu_q, \tag{54}$$

$$y_h^* = (1-\chi)y_h, \qquad y_q^* = \chi y_q. \tag{55}$$

Quantities corresponding to leptons are not affected by the ratio of the two baryonic components in the mixed phase.

The mixed phase extends over those densities $n_{\rm B}$ for which $0 \le \chi(n_{\rm B}) \le 1$. In contrast to the crossover case where S operates at *all* densities, χ is active only when the above condition is satisfied. Moreover, in the case of a Gibbs construction of the first-order phase transition scenario, χ and y_i are treated on an equal footing with no prior assumptions regarding their density dependence, whereas in the crossover scenario, S has a definitive functional form which the particle fractions must be adjusted to fit. As a consequence, even though both χ and S describe the quark-to-baryon fraction, the former is a quantity for which we solve while the latter acts as a constraint replacing the Gibbs condition for mechanical equilibrium.

The sound speeds are obtained following the prescription outlined in the previous subsection. Alternatively, the adiabatic sound speed in the mixed phase can be calculated from the corresponding ones in the pure hadronic and quark phases separately according to Ref. [8]

$$\frac{1}{c_{\rm ad}^{*2}} = \frac{1-\chi}{c_{{\rm ad},H}^2} + \frac{\chi}{c_{{\rm ad},Q}^2}. \tag{56}$$

VI. RESULTS

We turn now to present results based on calculations of the crossover EOS, associated NS properties, the two sound speeds and the resulting g-mode frequencies. For contrast, results corresponding to pure hadronic matter and those for a first-order phase transition treated using the Gibbs construction are also presented.

TABLE I. Parameter sets for the EOSs used in this work.

Model	Parameter	XOA	XOB	XOC	Units
ZL	a_0	−96.64	−90.39	−96.64	MeV
	b_0	58.85	52.60	58.85	MeV
	γ	1.40	1.446	1.40	
	a_1	−26.06	−232.78	−28.15	MeV
	b_1	7.34	212.46	7.83	MeV
	γ_1	2.45	1.1	3.5	
vMIT	m_u	5.0	5.0	5.0	MeV
	m_d	7.0	7.0	7.0	MeV
	m_s	150.0	150.0	150.0	MeV
	a	0.20	0.23	0.15	fm^2
	$B^{1/4}$	180.0	180.0	180.0	MeV
KW	μ_0	1.8	1.8	1.8	GeV

A. EOS and structural properties of NSs

To construct crossover models, we have chosen the parameter values shown in Table I, labeled as XOA, XOB and XOC, for the parametrization of the EOSs used in this work.[5] These sets of parameters correspond to the nuclear and neutron-star properties shown in Table II.

For XOA, all values are within 1-σ deviations of empirical/observational constraints discussed below. While XOB and XOC do not perform as well, they are used here to illustrate some important physics related to the behavior of the g-mode frequency. Specifically, with XOB we investigate g-mode frequency features corresponding to a sound-speed peak due to proton disappearance, whereas in XOC the peak in the speed of sound is not related to a change in the number of degrees of freedom. Models labeled ZL (nucleons only) and Gibbs (nucleons plus quarks with a Gibbs construction) use the appropriate parameters of XOA.

We wish to note that the values of the symmetry energy S_v and its slope L at $n_{\rm sat}$ used in our work (see Table II) lie in the range $\simeq 31 \pm 2$ MeV and $\simeq 51 \pm 11$ MeV, respectively, recommended in Ref. [24]. These values led to the bounds on the radius of a 1.4 $M_\odot$ star to be $R_{1.4} \simeq 12 \pm 1$ km.

Interpretations of the recent PREX-II experiment carried out at the Jefferson Lab (JLab) measuring the neutron skin thickness of ^{208}Pb [29], $R_{\rm skin}^{^{208}{\rm Pb}} = 0.283 \pm 0.071$ fm, however, widely vary in their inferences of the appropriate values of S_v and L to be used. For example, Reed *et al.* [30], using relativistic mean-field theory calculations to analyze the JLab data, conclude that $S_v = 38.1 \pm 4.7$ MeV and $L = 106 \pm 37$ MeV, values that are significantly higher

[5]The method to determine the constants for the ZL parametrization is described in Refs. [8,16].

TABLE II. Nuclear and neutron-star properties corresponding to the parametrizations shown in Table I. The symbols refer to $n_{\rm sat}$: nuclear saturation density, E_0: energy per particle at $n_{\rm sat}$, K_0: compression modulus of symmetric nuclear matter at $n_{\rm sat}$, S_v: symmetry energy at $n_{\rm sat}$, L: slope of $S(n)$ at $n_{\rm sat}$, $n^{\beta}_{\mu,\rm on}$: onset density of muons, $n^{\beta}_{\mu,\rm off}$: turnoff density of muons, and $n^{\beta}_{p,\rm off}$: turnoff density of protons. Quantities related to neutron stars are R: radius, M: mass, $\beta = GM/Rc^2$: compactness, n_c: central density, p_c: central pressure, ε_c: central energy density, Λ: dimensionless tidal deformability, $c^2_{\rm eq}$: squared equilibrium sound speed, and $c^2_{\rm ad}$: squared adiabatic sound speed. The subscripts 1.4 and max denote the masses of stars in $M_\odot$.

Property	XOA	XOB	XOC	ZL	Gibbs	Units
$n_{\rm sat}$	0.16	0.16	0.16	0.16	0.16	$\rm fm^{-3}$
E_0	−16.0	−16.0	−16.0	−16.0	−16.0	MeV
K_0	250.0	260.0	250.0	250.0	250.0	MeV
S_v	31.6	30.0	30.0	31.6	31.6	MeV
L	43.0	70.0	65.0	43.0	43.0	MeV
$n^{\beta}_{\mu,\rm on}$	0.13	0.15	0.14	0.13	0.13	$\rm fm^{-3}$
$n^{\beta}_{\mu,\rm off}$	1.39	0.77	1.67	⋯	1.32	$\rm fm^{-3}$
$n^{\beta}_{p,\rm off}$	⋯	0.88	⋯	⋯	⋯	$\rm fm^{-3}$
$R_{1.4}$	12.4	12.4	13.8	12.4	12.4	km
$\beta_{1.4}$	0.167	0.166	0.150	0.166	0.166	
$n_{c,1.4}/n_{\rm sat}$	2.64	3.16	1.96	2.64	2.68	
$p_{c,1.4}$	60.2	73.6	41.7	60.0	69.8	MeV $\rm fm^{-3}$
$\varepsilon_{c,1.4}$	424.7	518.4	316.7	424.9	436.3	MeV $\rm fm^{-3}$
$\Lambda_{1.4}$	428.9	426.7	841.3	430.1	421.2	
$(c^2_{\rm eq})_{c,1.4}$	0.398	0.331	0.294	0.397	0.406	c^2
$(c^2_{\rm ad})_{c,1.4}$	0.429	0.331	0.497	0.426	0.528	c^2
$R_{M_{\rm max}}$	11.5	10.4	13.0	11.1	11.2	km
$M_{\rm max}$	2.11	2.04	2.13	2.23	2.08	$M_\odot$
$\beta_{\rm max}$	0.270	0.289	0.242	0.295	0.275	
$n_{c,\rm max}/n_{\rm sat}$	5.83	7.38	4.70	6.14	6.32	
$p_{c,\rm max}$	362.7	696.1	213.4	577.0	457.7	MeV $\rm fm^{-3}$
$\varepsilon_{c,\rm max}$	1142.9	1549.5	886.8	1202.4	1264.9	MeV $\rm fm^{-3}$
$\Lambda_{\rm max}$	13.8	6.4	30.1	6.2	11.1	
$(c^2_{\rm eq})_{c,\rm max}$	0.426	0.566	0.316	0.767	0.576	c^2
$(c^2_{\rm ad})_{c,\rm max}$	0.507	0.818	0.353	0.889	0.653	c^2

than those deduced in earlier works. Furthermore, the bound $R_{1.4} > 13.25$ km was found there. Reinhard *et al.* [31], use covariant relativistic mean-field theory (with density-dependent couplings) and nonrelativistic energy functionals to analyze the PREX-II data and combine it with the dipole polarizability data of ^{208}Pb to arrive at $S_v = 32 \pm 1$ MeV and $L = 54 \pm 8$ MeV. In addition, these authors obtain $R^{^{208}\rm Pb}_{\rm skin} = 0.19 \pm 0.02$ fm in accord with earlier deductions. Similar results are obtained by Essick *et al.* [32] who report $S_v = 34 \pm 3$ MeV, $L = 58 \pm 18$ MeV and $R^{^{208}\rm Pb}_{\rm skin} = 0.19^{+0.03}_{-0.04}$ fm from a nonparametric EOS coupled with Gaussian processes. Combining recent mass and radius measurement from radio and x-ray data from *NICER*, Biswas [33] finds $R^{^{208}\rm Pb}_{\rm skin} = 0.20 \pm 0.05$ fm and $R_{1.4} = 12.75^{+0.42}_{-0.54}$ km using nuclear EOSs with piecewise polytrope parametrization. Given the fluid state of theoretical inferences from the analysis of JLab data, we have opted to stick with the values used in Table II.

Figure 1 shows mass versus radius ($M - R$) curves for all the models considered along with the recent constraints

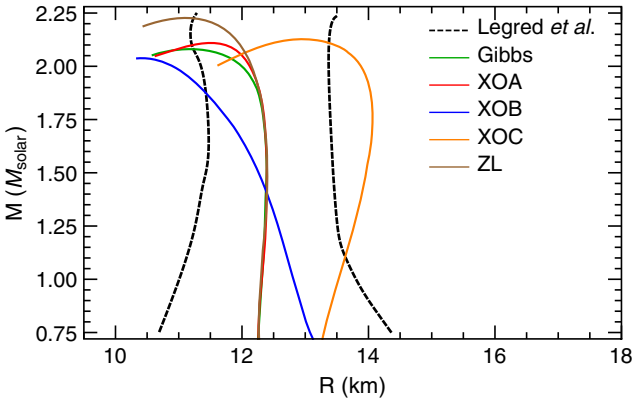

FIG. 1. Neutron-star $M - R$ curves for the various EOS models used in this work. The black, dashed lines represent the 90% confidence level constraints extracted from recent radio, x-ray, and gravitational-wave observations by Legred *et al.* [34]. Models corresponding to the "A" parameter set fit these constraints well with differences between the three depending on the order of the transition to quark matter or the lack thereof. While stars with $M \leq 1.8\ M_\odot$ using model XOB are within the constraints, with model XOC only stars close to the maximum mass satisfy the Legred *et al.* constraints.

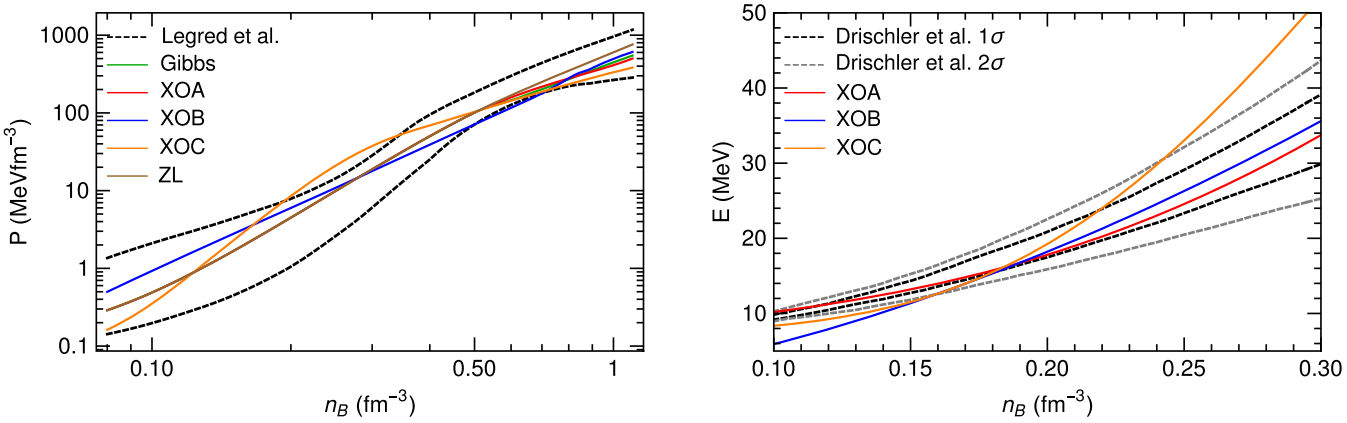

FIG. 2. Left panel: pressure versus baryon density as obtained by the assorted EOSs used herein compared with the astrophysical constraints of Legred *et al.* [34] (in black, dashed lines). All parametrizations meet these constraints successfully with the exception of XOC which fails to stay in the allowed region around $2.0n_{\rm sat}$, where $n_{\rm sat} = 0.16$ fm^{-3}. Right panel: energy per particle versus baryon density of beta-equilibrium matter for the various EOSs used in this work compared with the 1-σ and 2-σ constraints from Drischler *et al.* [23] obtained in a chiral EFT framework. Results corresponding to Gibbs and ZL are not shown because, over the range of densities displayed, they are identical to XOA. Only XOA remains within the 2-σ constraints of [23] up to $\sim 2.0n_{\rm sat}$.

obtained by Legred *et al.* [34], which combined available observations including the radio mass measurements of PSR J0348 + 0432 and J0470 + 6620 [35–37], the mass and tidal deformability measurements of GW170817 and GW190425 [38–40], and the x-ray mass and radius constraints from latest *NICER* measurements of J0030 + 0451 and J0470 + 6620 [41–44]. The constraints of Legred *et al.* were obtained by using the hierarchical inference [45] and a nonparametric survey through Gaussian processes conditioned on existing EOS models in the literature [46–48].

The left panel of Fig. 2 displays results of the pressure versus baryon number density ($P - n_{\rm B}$) relation for the various models used in the present work, in contrast to those inferred from Ref. [34] mentioned above (the black dashed boundaries, adapted from their Fig. 4). To provide a comparison, results of energy versus density E vs $n_{\rm B}$ of β-equilibrated NSM are shown in the right panel of Fig. 2, together with those for NSM from the chiral effective theory calculations of Ref. [23] where 1-σ and 2-σ error estimates up to $\sim 2.0n_{\rm sat}$ were provided. Although not shown, we also find that results of the crossover, ZL and Gibbs models for $P - n_{\rm B}$ and E vs $n_{\rm B}$ are consistent with microscopic Greens' function calculations of Gandolfi *et al.* [49].

The squared adiabatic and equilibrium sound speeds $c^2_{\rm ad}$ and $c^2_{\rm eq}$ versus baryon density $n_{\rm B}$ are shown in the left and right panels of Fig. 3, respectively. Both $c^2_{\rm ad}$ and $c^2_{\rm eq}$ increase monotonically with $n_{\rm B}$ for the ZL model in which nucleons are the only baryons. The nonmonotonic behaviors of the other curves are due to admixtures of nucleons and quarks in the baryon sector. The $c^2_{\rm eq}(n_{\rm B})$ for the Gibbs model suddenly drops (rises) at the onset (end) of the mixed phase (the latter not shown in the figure), whereas $c^2_{\rm ad}(n_{\rm B})$ varies smoothly. Results for the crossover models XOA and

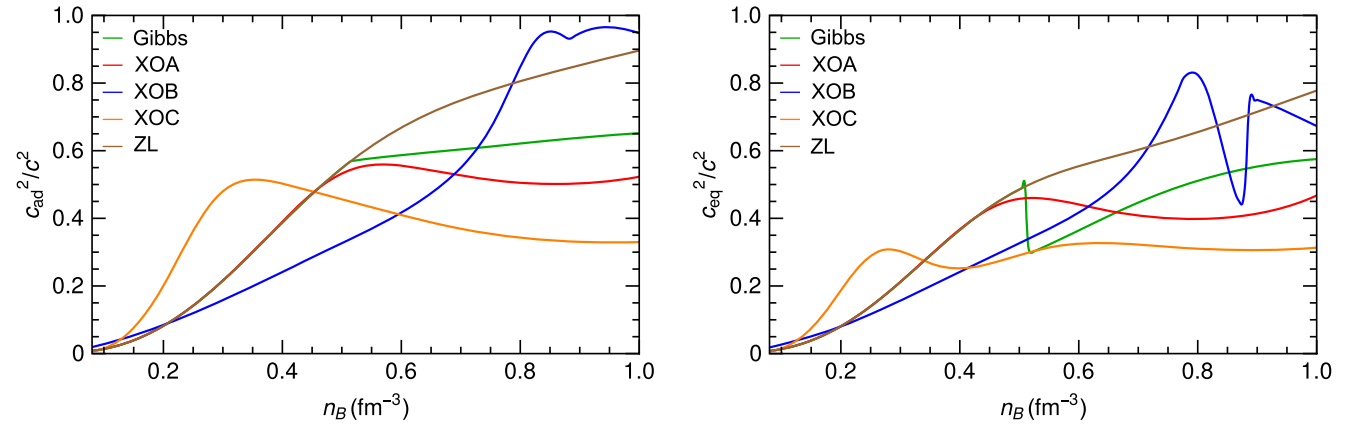

FIG. 3. Left panel: the squared adiabatic sound speed $c^2_{\rm ad}$ as a function of the baryon density $n_{\rm B}$. Right panel: the squared equilibrium sound speed $c^2_{\rm eq}$ as a function of the baryon density $n_{\rm B}$.

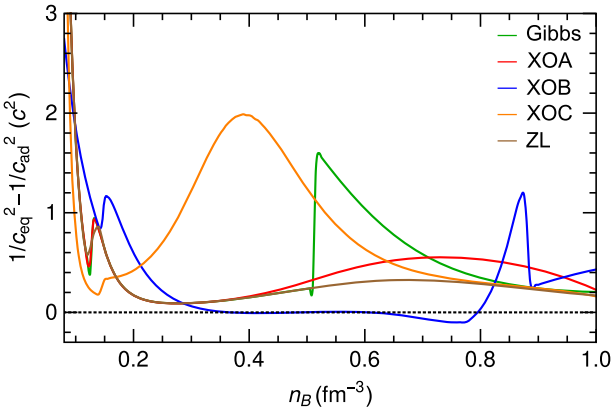

FIG. 4. Difference between the inverse-squared sound speeds versus the baryon number density. The peaks in the vicinity of n_{sat} correspond to muon appearance and are present in all models. The peak at $\sim 3n_{sat}$ for Gibbs occurs at the onset of the mixed phase which extends beyond the densities shown here. The peak around $5.5n_{sat}$ for XOB is the combined effect of muon and proton disappearance in this model. On the other hand, the peak at $\sim 2.5n_{sat}$ for XOC results from inflection points in the quark and neutron fractions.

XOC are similar in structure, whereas those for XOB show more structure at large n_B due to the disappearance of protons. With the exception of model XOB, $c_{ad}^2 > c_{eq}^2$ for all other models at all n_B.

Figure 4 shows the difference of the inverses of the adiabatic and equilibrium sound speeds, $\Delta(c^{-2}) \equiv 1/c_{eq}^2 - 1/c_{ad}^2$ as a function of the baryon density. This quantity is particularly important in the context of g modes because it enters directly in the calculation of the Brunt-Väisälä frequency (discussed in more detail in the next section).

A comparison between this figure and Figs. 5–7, which show the particle fractions corresponding to the three crossover models used in this work, reveals a direct correlation between sharp maxima in the former and particle appearance/disappearance in the latter. Smooth

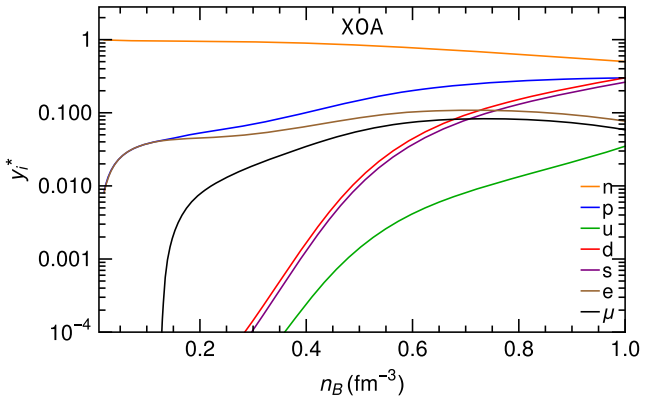

FIG. 5. Particle fractions of the crossover model XOA versus baryon density. Quarks are still present below 0.3 fm^{-3} but at two orders of magnitude less than what is shown here.

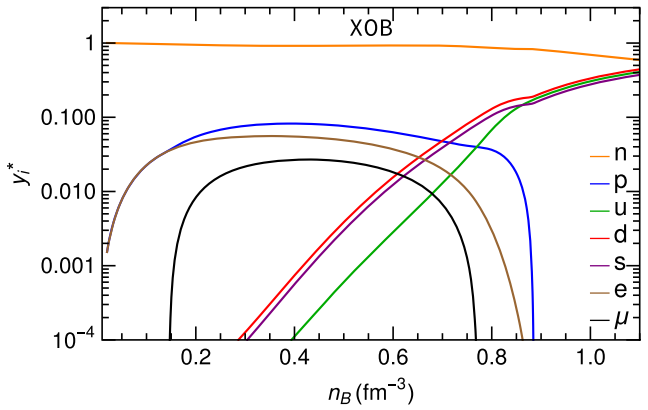

FIG. 6. Particle fractions of model XOB versus baryon density. Muons drop out of the system at 0.77 fm^{-3} and protons at 0.88 fm^{-3} leading to a sharp peak in the adiabatic sound speed (cf. Fig. 4). Electrons are still present above 0.85 fm^{-3} but at two orders of magnitude less than what is shown here.

maxima, such as those exhibited by XOA around 0.7 fm^{-3} and XOC around 0.4 fm^{-3}, reflect nonmonotonic behaviors in the slopes of the quark and the neutron fractions. Also worth noting is that, in the present framework and with the chosen parametrizations, quarks are never the dominant contributors to the baryon density for densities relevant to neutron stars.

Consequently, the contributions of quarks to the total baryon number as well as the total mass of the star (both baryonic and gravitational) are rather small in the models considered, as shown in Table III for stars with gravitational mass $M = 2\ \mathrm{M}_\odot$. These are straightforwardly calculated as follows: the solution of the Tolman–Oppenheimer–Volkoff (TOV) equations [73,74] gives, among other things, the baryon density as a function of the star's radius, $n_B(r)$. The quark particle fractions as functions of the baryon density are obtained from the β-equilibrated equivalents of Eqs. (28) and (55) for the KW and Gibbs cases, respectively.

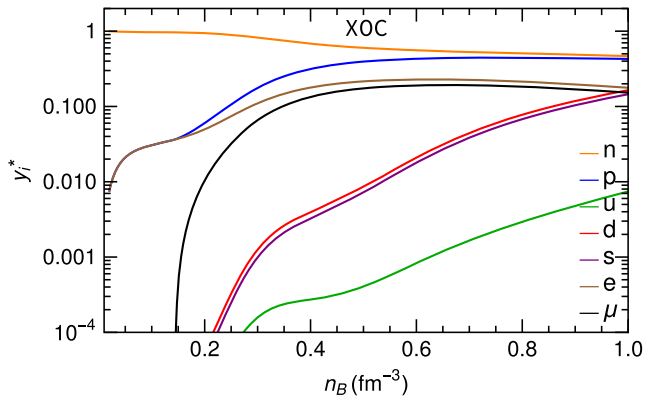

FIG. 7. Particle fractions of model XOC versus baryon density. The inflectionary behavior of the quark and neutron fractions around 0.4 fm^{-3} is responsible for the broad peak behavior of XOC occurring in Fig. 4.

TABLE III. Various representations of the quark content of 2 $M_\odot$ NSs corresponding to the Gibbs and the three crossover models in this paper. The symbols are M_B: the total baryonic mass, Y_Q^{bar}: contribution of quarks to the total baryon number/total baryon number, Y_Q^{part}: quark particle number/total particle number, Y_Q^{nuc}: quark particle number/nucleon number, M_Q^B/M_B: contribution of quarks to the total baryonic mass/total baryonic mass, and M_Q^G/M_G: contribution of quarks to the total gravitational mass/total gravitational mass.

Model	M_B ($M_\odot$)	Y_Q^{bar} ($\times 10^{-2}$)	Y_Q^{part} ($\times 10^{-2}$)	Y_Q^{nuc} ($\times 10^{-2}$)	M_Q^B/M_B ($\times 10^{-2}$)	M_Q^G/M_G ($\times 10^{-2}$)
XOA	2.31	0.35	1.03	1.04	0.35	0.50
XOB	2.33	2.15	6.18	6.58	2.15	3.04
XOC	2.29	0.06	0.19	0.19	0.06	0.09
Gibbs	2.35	1.91	5.53	5.85	1.91	2.89

Explicitly, $y_q(r) = y^*_{q,\beta}[n_B(r)]$. For the quark baryon fraction at each radius we divide this by 3. The quark particle densities are then $n_q(r) = y_q(r) n_B(r)$.The baryon number due to quarks of all species $q = u, d, s$ in the star is given by the integral

$$N_Q = 4\pi \int_0^R dr r^2 \frac{\sum_q n_q(r)/3}{[1 - 2GM(r)/r]^{1/2}}. \tag{57}$$

Here, $M(r)$ is the total gravitational mass of the star as a function of its radius r, also given by the solution of the TOV equations. Therefore, the amount of baryonic mass in the star provided by quarks is $M_Q^B = m_H N_Q$ [50]. For the quark gravitational mass we begin by calculating the quark energy density as a function of the radius according to $\varepsilon_Q(r) = \varepsilon^*_{Q,\beta}[n_B(r)]$, where $\varepsilon^*_Q = -SP_Q + \sum_q n^*_q \mu_q$. Afterwards, we perform the integral $M_Q^G = 4\pi \int_0^R dr r^2 \varepsilon_Q(r)$.

Specifically, in model XOA, quarks contribute less than 0.5% of the total baryon number, about 1% of particles in its 2 $M_\odot$ stars are quarks and they are responsible for around 0.35% (0.5%) of the total baryonic (gravitational) mass of the star. For XOB and Gibbs models, quarks contribute about 2% of the total baryon number, over 5% of the total particle number, and 2% (3%) of the total baryonic (gravitational) mass of the respective 2 $M_\odot$ stars. In model XOC, quarks are, for all intents and purposes, irrelevant. As noted before, such a clean separation may not be possible in treatments that intermingle hadron/nucleon and quark interactions.

B. Sound speeds and the Brunt-Väisälä frequency

Having outlined the thermodynamics of the multicomponent system and the specific models employed in our study of the smooth crossover transition in neutron stars, we turn now to the calculation of the star's g-mode frequencies. Our main goal is to compare the behavior of the g-mode frequencies in the crossover model with those in the Gibbs mixed phase. The g-mode frequencies [$\nu_g = \omega/(2\pi)$] and normalized amplitudes for the radial and tangential parts of the fluid perturbation (ξ_r and ξ_h, respectively) are estimated within the relativistic Cowling approximation (see below) by computing numerical solutions to the following equations of motion for fluid variables U, V [8]

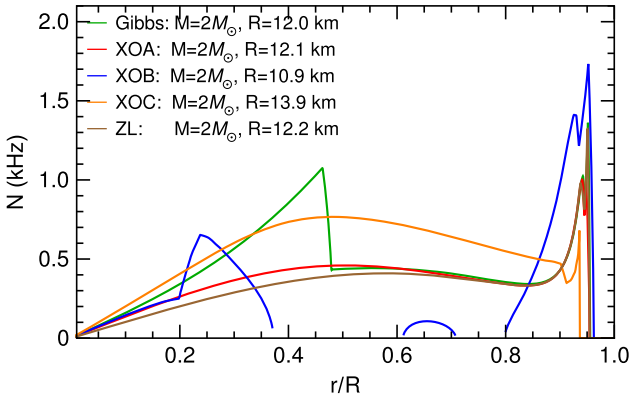

FIG. 8. The Brunt-Väisälä frequency in a hybrid star of mass 2.0 $M_\odot$ for the Gibbs and crossover models. The Brunt-Väisälä frequency for the "good" crossover model XOA is very similar to the nucleonic ZL EOS (which includes muons), whereas the Gibbs model shows a distinct peak corresponding to the rapid onset of quark matter. Parameters for the nuclear and quark EOSs are as in Table I.

$$\frac{dU}{dr} = \frac{g}{c_{ad}^2} U + e^{\lambda/2} \left[\frac{l(l+1)e^{\nu}}{\omega^2} - \frac{r^2}{c_{ad}^2} \right] V,$$
$$\frac{dV}{dr} = e^{\lambda/2 - \nu} \frac{\omega^2 - N^2}{r^2} U + g\Delta(c^{-2}) V, \tag{58}$$

which are simplified forms of the original perturbation equations [4,51,52]. In Eq. (58), $U = r^2 e^{\lambda/2} \xi_r$, $V = \omega^2 r \xi_h = \delta P/(\varepsilon + P)$, $\Delta(c^{-2}) = c_{eq}^{-2} - c_{ad}^{-2}$ and λ and ν are metric functions. The scale of the mode frequency is set by the Brunt-Väisälä frequency

$$N^2 = g^2 \Delta(c^{-2}) e^{\nu - \lambda}, \tag{59}$$

where $g = -\nabla P/(\varepsilon + P)$.

The relativistic Cowling approximation neglects the back reaction of the gravitational potential by excluding metric perturbations that must accompany matter perturbations in a general relativistic treatment [53–58]. It reduces the number and complexity of the equations we have to solve, while providing results for g-mode frequencies that are accurate at the few % level [59]. Details on the solution methods for Eq. (58) and relevant boundary conditions are provided in Ref. [8].

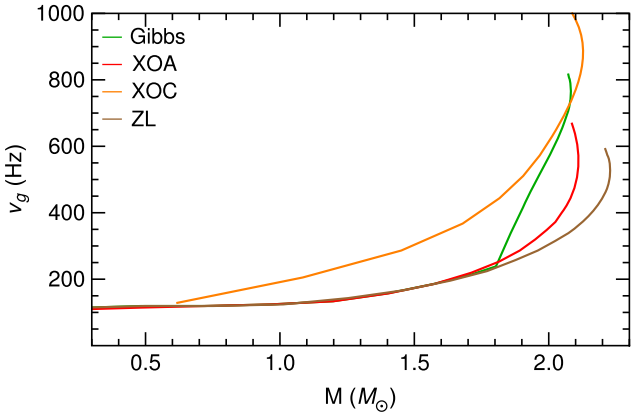

FIG. 9. The g-mode frequency as a function of the stellar mass in the Gibbs, crossover, and ZL models. Parameters for the nuclear and quark EOSs are as in Table. I. The g modes corresponding to XOB are unstable, and therefore this model is excluded from the present and the next two figures.

Figure 8 is a comparison of the Brunt-Väisälä frequency in the three models considered in this work. The crossover model, where quarks are always present in the core EOS, albeit in minuscule fractions, resembles the purely nucleonic ZL EOS in this respect, while the sudden onset of quarks in the Gibbs model is clearly imprinted in the form of a sharp peak. Quarks enter at a density $n_B \simeq 0.514$ fm^{-3} corresponding to $r/R = 0.473$ ($r = 0$ at the center) in the Gibbs model. As a consequence of the difference of sound speeds being negative in distinct density regimes for XOB (Fig. 4), the corresponding Brunt-Väisälä frequency is imaginary, implying an instability to convection.[6] However, convection is absent at zero temperature; therefore these regions are unphysical and can play no role in the global g-mode spectrum. Accordingly, XOB is omitted from Figs. 9–11.

Figure 9 compares the g-mode frequency, $\nu_g = \omega/(2\pi)$, for the crossover and Gibbs models. While XOA and XOC are very similar to the nucleonic ZL EOS (which includes muons), the Gibbs model shows a distinctly rising spectrum corresponding to the rapid onset of quark matter. These findings are consistent with the result for the Brunt-Väisälä frequency in Fig. 8 and the conclusions in paper I. In the crossover model XOB, protons disappear above some critical density. In contrast to the smooth behavior of g-mode frequencies in XOA and XOC, the sudden disappearance of protons in XOB produces a sharp rise in the spectrum akin to the Gibbs case but renders g modes to become unstable (not shown in Fig. 9), confirming that dramatic changes in the g-mode frequency require the *appearance or disappearance of a (strongly interacting) particle species, not merely a smooth change in composition*. This is why, except for extreme parameter choices, crossover models will not show the g-mode feature resulting from the presence of quarks that Gibbs models do.

[6]This feature could be an artifact of the Cowling approximation, but will likely be absent in the solution of the full general relativistic treatment [53–58] of the g mode in which c_{eq}^2 does not enter explicitly.

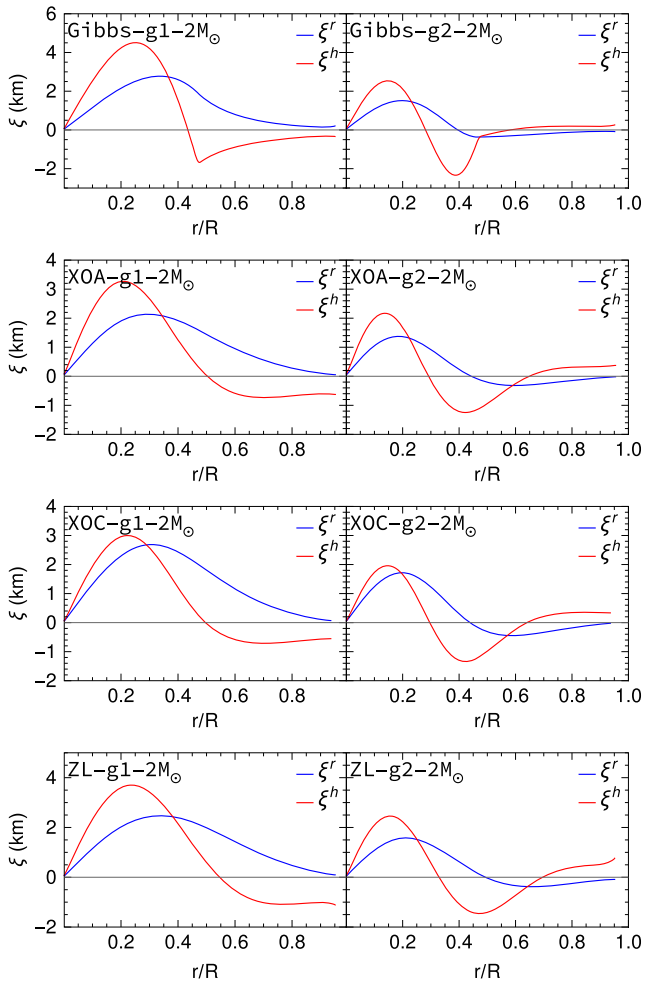

FIG. 10. Amplitudes of the radial (r) and transverse (h) components of the g-mode displacement (eigenfunctions) as a function of distance from the center for the ZL, XOA, XOC and Gibbs EOSs for a ~2 $M_\odot$ star. The order of the mode (g1 is fundamental, g2 is overtone) is indicated in the legend in the panels.

The panels in Fig. 10 show the comparison of the core g-mode amplitude between the three chosen models (ZL, crossover and Gibbs). The radial component ξ_r of the fundamental mode (labeled "g1" in the panels) has no nodes in the core, while the radial part of the first overtone (labeled "g2") has one, as expected. The horizontal component ξ_h has one more node than the corresponding radial component of the same order. The larger amplitude of ξ_h relative to ξ_r indicates that the g mode is dominated by transverse motion of the perturbed fluid. While there is little difference between the ZL and crossover models in the profile of these eigenfunctions, the Gibbs case is markedly different. Its amplitude relative to the other two is larger,

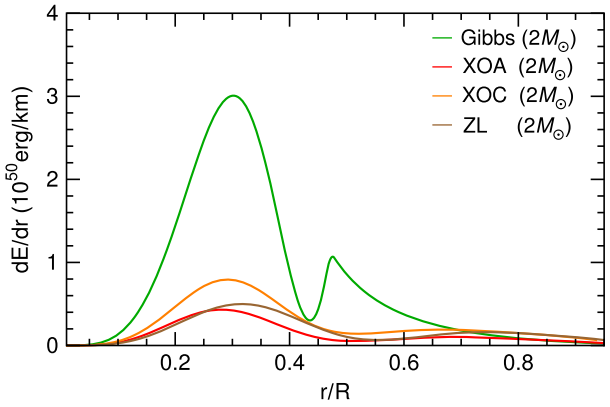

FIG. 11. Energy/unit distance of the fundamental g mode as a function of distance from the center for the ZL, XOA, XOC, and Gibbs EOS for a ~2 $M_\odot$ star. Note that the mode energies in the ZL and crossover cases are scaled up by a factor of 10 for the purpose of comparison.

and it changes abruptly upon the onset of quark matter in the core.

The energy per unit radial distance dE_T/dr contained in the oscillatory motion corresponding to a frequency ω is given in terms of the amplitude as [51]

$$\frac{dE_T}{dr} = \frac{\omega^2 r^2}{2}(\varepsilon + P)e^{(\lambda-\nu)/2}[\xi_r^2 e^{\lambda} + l(l+1)\xi_h^2]. \quad (60)$$

Figure 11 shows the comparison of the core g-mode energy/unit distance for the three chosen models (ZL, crossover and Gibbs) for a ~2 $M_\odot$ star. The typical scale of the energy/unit distance deep in the core is approximately 10^{50} ergs/km for the ZL and crossover models, while it is of order 10^{51} ergs/km for the Gibbs case. While the profiles are similar for the first two, the mode energy in the Gibbs case is overwhelmingly larger in the core, once quark matter appears. Thus, both the frequency and the amplitude (and hence the energy) of the core g mode is strongly amplified in quark matter in comparison to nucleonic matter or weaker forms of the phase transition. This can have bearing on the gravitational wave detection of g modes excited in neutron star mergers as discussed below.

C. Discussion

The results in the previous subsection raise some points that are noteworthy. In particular, they highlight the relation between the behaviors of the speeds of sound and of the particle concentrations, and the spectrum of the g-mode signal. Thus, the latter becomes a diagnostic which distinguishes nucleonic and hybrid matter *as well as* the Gibbs and crossover transitions.

Peaks in the sound-speed difference $\delta c \equiv c_{\rm ad}^2 - c_{\rm eq}^2$, and the difference of the inverses $\Delta(c^{-2}) \equiv 1/c_{\rm eq}^2 - 1/c_{\rm ad}^2$ occur when particles appear or disappear [i.e., when the number of degrees of freedom (DOF) of the system changes] and when the particle concentrations $y_i(n_{\rm B})$ are not monotonic or have inflection points (i.e., their first or second derivatives with respect to $n_{\rm B}$ change sign).

The introduction or removal of a particle species from the system occurs when the relevant chemical potential either exceeds or falls below its rest mass threshold while maintaining charge neutrality. Whereas the functional form of the y_i's depends on the parametrization of the EOS, a change in the number of DOFs also leads to nonmonotonic or inflectional behavior to the concentrations of particles already present in the system. Thus, in some sense, specific choices of the EOS parameters can mimic aspects of the emergence of new particles that are relevant to the sound speeds.

Signals of g mode with a characteristic fast rise in its frequency (such as those corresponding to Gibbs shown in Fig. 9 and XOB for which the g mode becomes unstable) can occur only when particle species enter or leave the system. In such cases, the peaks in $\Delta(c^{-2})$ are sharp and asymmetric: vertical rise and quasi-Lorentzian decay for appearance (see Fig. 4, Gibbs), and quasi-Lorentzian rise and vertical drop for disappearance (XOB); whereas peaks due to parametrizations resemble symmetric Gaussians (XOC). Therefore, this kind of signal cannot be produced by quarks in matter with a smooth crossover because quarks are always present: their concentrations are vanishingly small at lower densities but never identically zero.

It is, however, possible to parametrize the hadronic EOS such that, in β-equilibrated crossover matter, protons exit the system. The magnitude of the peak of $\Delta(c^{-2})$ *appears* to be proportional to the number of remaining DOFs (smallest in PNM; largest in $n-uds-e$ matter). This produces g-mode frequency spectra similar to those found in matter with a Gibbs construction. So, although quarks are not directly responsible for this effect, they do serve the purpose of amplifying it.

For the specific case of crossover model XOB, a rather extreme parametrization ($K = 260$ MeV, $S_v = 30$ MeV, $L = 70$ MeV, $\gamma_1 = 1.1$) was required for the proton disappearance while also meeting neutron-star constraints and having a peak at low-enough densities to be relevant. Consequently, the tentative conclusion is that hyperons or a first-order transition into quark matter through Gibbs construction are more likely to cause a distinctive peak in the Brunt-Väisälä frequency than a crossover transition; nevertheless, the latter remains a viable, if improbable, option.

It is pertinent to mention that we have not performed calculations for first-order transitions with a Maxwell construction, which assume a sufficiently large surface tension between the pure hadronic and quark phases in bulk separated by a sharp boundary. It has been shown that in such cases, g modes always vanish when the perturbed fluid element adjusts instantaneously (i.e., a very rapid

conversion) to maintain thermodynamic equilibrium, but can arise if the microscopic phase conversion at the interface is slow enough, leading to distinctive features on the extended hybrid branch of NSs [60,61]. Such g modes associated with a discontinuity in density ("*discontinuity g* modes," which are different from the "*compositional g* modes" that we consider) has been widely studied in the literature; see e.g., extensive discussions in Refs. [62–66].

VII. SUMMARY AND CONCLUSIONS

The main objectives of this work were to examine g-mode frequencies in a smooth crossover scenario of the hadron-to-quark transition, and to compare them with those of a first-order transition treated using Gibbs and Maxwell constructions in paper I [8]. For the crossover model, we chose the recent approach adopted by Kapusta and Welle [2], who constructed an EOS for PNM that resembled the smooth crossover observed in lattice calculations at finite temperatures. We have generalized their approach to β-equilibrated NSM so that comparisons with the results of paper I could be made. To describe nucleons, we used the ZL parametrization [16] which reproduces near-saturation laboratory data as well as results of chiral EFT calculations [22,23] up to $\sim 2.0 n_{\rm sat}$. For quark matter we used the vMIT model [25] with repulsive interactions. Results of our crossover EOSs tally with observational findings of the radii of $\sim$1.4 and $\sim$2.0 $M_\odot$ NSs [41–44]. Calculations of the equilibrium and adiabatic speeds of sound were performed following the procedures developed in paper I. Our work here is focused on zero temperature and does not consider superfluidity in either nucleons or quarks. Inclusion of these effects will be taken up in a future work.

The results of the amplitudes of the g-mode frequencies and their associated amplitudes of the gravitational energy radiated for the chosen hadron-to-quark crossover models lie between those of the first-order phase transitions that employ Maxwell and Gibbs constructions. For the case of the Maxwell construction, the transition region is devoid of g-mode frequencies as the equilibrium and adiabatic sound speeds both vanish. Consequently, g-mode oscillations are permitted only for the pure nucleonic and quark phases. Their amplitudes in these regions are, however, rather small. In contrast, the mixed phase in the case of the Gibbs construction yields amplitudes of g-mode frequencies and the energy radiated that are significantly larger than those of the crossover model.

We note that g-mode frequencies can be exceptionally large in the presence of superfluidity ($\approx$750 Hz for a hyperonic star [67] and $\approx$450 Hz for a nucleonic star [68,69]), similar to the results for the Gibbs mixed phase. However, the reason for the enhancement in the two cases is different. In the case of superfluidity, the temperature-dependence of the entrainment terms serves to increase the g-mode frequency at typical neutron star temperatures, while in the Gibbs case, the enhancement is purely composition dependent. A study of resonant excitations of such superfluid modes in coalescing neutron star binaries [70] suggests that the amplitude of these modes is weaker by a factor of 20 or so, compared to modes from the normal fluid. Note that the g modes we discuss here are also higher in frequency compared to the low-frequency g modes ($\sim$50 Hz) that might strain the neutron star crust to breaking point and lead to precursor flares in gamma-ray bursts [71].

The relatively larger frequency, amplitude and energy of the g mode in the Gibbs case inferred from Figs. 9–11 have observational implications for gravitational waves from neutron star mergers. It has been established that g modes can couple to tidal forces and draw energy and angular momentum from the binary to the neutron star, leading to an accelerated merger and a concomitant phase shift in the gravitational waveform [6]. This coupling will be largest for the Gibbs case, with its higher energy at resonance, and also because higher resonance frequencies are excited later in the inspiral, when tidal forces are strongest. Estimates of the resulting phase shift were presented in paper I [Eq. (89)] and found to be comparable to that from g modes in ordinary neutron stars (due to longer merger times) within uncertainties arising from the value of the tidal coupling. As these uncertainties are reduced through improved theoretical calculations, the case of a hybrid star may be distinguished from an ordinary neutron star. We also infer from our results that were high-frequency g modes to be detected in upgraded LIGO and Virgo observatories, it would indicate a first-order phase transition akin to a Gibbs construction. In light of data from GW170817, lower bounds on the excitation of nonradial oscillations in binary mergers [72] affirm that a third generation network with its improved sensitivity and larger bandwidth can shed new light on the composition of the neutron star core.

ACKNOWLEDGMENTS

C. C. acknowledges support from the European Union's Horizon 2020 research and innovation program under the Marie Skłodowska-Curie Grant Agreement No. 754496 (H2020-MSCA-COFUND-2016 FELLINI). S. H. is supported by the National Science Foundation, Grant No. PHY-1630782, and the Heising-Simons Foundation, Grant No. 2017-228. P. J. is supported by the U.S. National Science Foundation Grant No. PHY-1913693. M. P.'s research was supported by the Department of Energy, Grant No. DE-FG02-93ER40756.

[1] S. Borsanyi, G. Endrodi, Z. Fodor, A. Jakovac, S. D. Katz, S. Krieg, C. Ratti, and K. K. Szabo, J. High Energy Phys. 11 (2010) 077.
[2] J. I. Kapusta and T. Welle, Phys. Rev. C **104**, L012801 (2021).
[3] S. Han, M. A. A. Mamun, S. Lalit, C. Constantinou, and M. Prakash, Phys. Rev. D **100**, 103022 (2019).
[4] A. Reisenegger and P. Goldreich, Astrophys. J. **395**, 240 (1992).
[5] A. Reisenegger and P. Goldreich, Astrophys. J. **426**, 688 (1994).
[6] D. Lai, Mon. Not. R. Astron. Soc. **270**, 611 (1994).
[7] D. Lai, Mon. Not. R. Astron. Soc. **307**, 1001 (1999).
[8] P. Jaikumar, A. Semposki, M. Prakash, and C. Constantinou, Phys. Rev. D **103**, 123009 (2021).
[9] W. Wei, M. Salinas, T. Klähn, P. Jaikumar, and M. Barry, Astrophys. J. **904**, 187 (2020).
[10] V. Dexheimer, R. Negreiros, and S. Schramm, Phys. Rev. C **91**, 055808 (2015).
[11] G. Baym, T. Hatsuda, T. Kojo, P. D. Powell, Y. Song, and T. Takatsuka, Rep. Prog. Phys. **81**, 056902 (2018).
[12] K. Masuda, T. Hatsuda, and T. Takatsuka, Prog. Theor. Exp. Phys. **2013**, 073D01 (2013).
[13] K. Fukushima and T. Kojo, Astrophys. J. **817**, 180 (2016).
[14] T. Kojo, P. D. Powell, Y. Song, and G. Baym, Phys. Rev. D **91**, 045003 (2015).
[15] L. McLerran and S. Reddy, Phys. Rev. Lett. **122**, 122701 (2019).
[16] T. Zhao and J. M. Lattimer, Phys. Rev. D **102**, 023021 (2020).
[17] K. S. Jeong, L. McLerran, and S. Sen, Phys. Rev. C **101**, 035201 (2020).
[18] S. Sen and L. Sivertsen, Astrophys. J. **915**, 109 (2021).
[19] P. Papazoglou, D. Zschiesche, S. Schramm, J. Schaffner-Bielich, H. Stöcker, and W. Greiner, Phys. Rev. C **59**, 411 (1999).
[20] V. Dexheimer and S. Schramm, Astrophys. J. **683**, 943 (2008).
[21] V. A. Dexheimer and S. Schramm, Phys. Rev. C **81**, 045201 (2010).
[22] C. Drischler, R. J. Furnstahl, J. A. Melendez, and D. R. Phillips, Phys. Rev. Lett. **125**, 202702 (2020).
[23] C. Drischler, S. Han, J. M. Lattimer, M. Prakash, S. Reddy, and T. Zhao, Phys. Rev. C **103**, 045808 (2021); Private communication.
[24] J. M. Lattimer and Y. Lim, Astrophys. J. **771**, 51 (2013).
[25] R. O. Gomes, P. Char, and S. Schramm, Astrophys. J. **877**, 139 (2019).
[26] T. Klähn and T. Fischer, Astrophys. J. **810**, 134 (2015).
[27] A. Kurkela, P. Romatschke, and A. Vuorinen, Phys. Rev. D **81**, 105021 (2010).
[28] A. Kurkela, E. S. Fraga, J. Schaffner-Bielich, and A. Vuorinen, Astrophys. J. **789**, 127 (2014).
[29] D. Adhikari *et al.* (PREX Collaboration), Phys. Rev. Lett. **126**, 172502 (2021).
[30] B. T. Reed, F. J. Fattoyev, C. J. Horowitz, and J. Piekarewicz, Phys. Rev. Lett. **126**, 172503 (2021).
[31] P.-G. Reinhard, X. Roca-Maza, and W. Nazarewicz, arXiv:2105.15050 [Phys. Rev. D (to be published)].
[32] R. Essick, I. Tews, P. Landry, and A. Schwenk, Phys. Rev. Lett. **127**, 192701 (2021).
[33] B. Biswas, Astrophys. J. **921**, 63 (2021).
[34] I. Legred, K. Chatziioannou, R. Essick, S. Han, and P. Landry, Phys. Rev. D **104**, 063003 (2021).
[35] E. Fonseca *et al.*, Astrophys. J. Lett. **915**, L12 (2021).
[36] H. T. Cromartie *et al.*, Nat. Astron. **4**, 72 (2020).
[37] J. Antoniadis *et al.*, Science **340**, 6131 (2013).
[38] B. Abbott *et al.* (LIGO Scientific and Virgo Collaborations), Phys. Rev. X **9**, 011001 (2019).
[39] B. Abbott *et al.* (LIGO Scientific and Virgo Collaborations), Phys. Rev. Lett. **119**, 161101 (2017).
[40] B. Abbott *et al.* (LIGO Scientific and Virgo Collaborations), Astrophys. J. Lett. **892**, L3 (2020).
[41] M. Miller *et al.*, Astrophys. J. Lett. **887**, L24 (2019).
[42] T. E. Riley *et al.*, Astrophys. J. Lett. **887**, L21 (2019).
[43] M. C. Miller *et al.*, Astrophys. J. Lett. **918**, L28 (2021).
[44] T. E. Riley *et al.*, Astrophys. J. Lett. **918**, L27 (2021).
[45] T. J. Loredo, AIP Conf. Proc. **735**, 195 (2004).
[46] P. Landry, R. Essick, and K. Chatziioannou, Phys. Rev. D **101**, 123007 (2020).
[47] P. Landry and R. Essick, Phys. Rev. D **99**, 084049 (2019).
[48] R. Essick, P. Landry, and D. E. Holz, Phys. Rev. D **101**, 063007 (2020).
[49] S. Gandolfi, J. Carlson, and S. Reddy, Phys. Rev. C **85**, 032801(R) (2012).
[50] N. K. Glendenning, *Compact Stars* (Springer, New York, 2012).
[51] P. N. McDermott, H. M. van Horn, and J. F. Scholl, Astrophys. J. **268**, 837 (1983).
[52] E. M. Kantor and M. E. Gusakov, Mon. Not. R. Astron. Soc. **442**, L90 (2014).
[53] K. S. Thorne and A. Campolattaro, Astrophys. J. **149**, 591 (1967).
[54] K. S. Thorne and A. Campolattaro, Astrophys. J. **152**, 673 (1968).
[55] L. Lindblom and S. L. Detweiler, Astrophys. J. Suppl. Ser. **53**, 73 (1983).
[56] S. Detweiler and L. Lindblom, Astrophys. J. **292**, 12 (1985).
[57] L. S. Finn, Mon. Not. R. Astron. Soc. **227**, 265 (1987).
[58] N. Andersson, K. D. Kokkotas, and B. F. Schutz, Mon. Not. R. Astron. Soc. **274**, 1039 (1995).
[59] P. Gregorian, Nonradial neutron star oscillations, Master's thesis, https://dspace.library.uu.nl/handle/1874/306758.
[60] J. P. Pereira, C. V. Flores, and G. Lugones, Astrophys. J. **860**, 12 (2018).
[61] L. Tonetto and G. Lugones, Phys. Rev. D **101**, 123029 (2020).
[62] H. Sotani, K. Tominaga, and K.-i. Maeda, Phys. Rev. D **65**, 024010 (2001).
[63] C. V. Flores and G. Lugones, Classical Quantum Gravity **31**, 155002 (2014).
[64] I. F. Ranea-Sandoval, O. M. Guilera, M. Mariani, and M. G. Orsaria, J. Cosmol. Astropart. Phys. 12 (2018) 031.
[65] M. C. Rodriguez, I. F. Ranea-Sandoval, M. Mariani, M. G. Orsaria, G. Malfatti, and O. M. Guilera, J. Cosmol. Astropart. Phys. 02 (2021) 009.
[66] S. Y. Lau and K. Yagi, Phys. Rev. D **103**, 063015 (2021).

[67] V. A. Dommes and M. E. Gusakov, Mon. Not. R. Astron. Soc. **455**, 2852 (2016).
[68] M. E. Gusakov and E. M. Kantor, Phys. Rev. D **88**, 101302(R) (2013).
[69] A. Passamonti, N. Andersson, and W. C. G. Ho, Mon. Not. R. Astron. Soc. **455**, 1489 (2016).
[70] H. Yu and N. N. Weinberg, Mon. Not. R. Astron. Soc. **464**, 2622 (2017).
[71] H.-J. Kuan, A. G. Suvorov, and K. D. Kokkotas, Mon. Not. R. Astron. Soc. **506**, 2985 (2021).
[72] G. Pratten, P. Schmidt, and T. Hinderer, Nat. Commun. **11**, 2553 (2020).
[73] R. C. Tolman, Phys. Rev. **55**, 364 (1939).
[74] J. R. Oppenheimer and G. M. Volkoff, Phys. Rev. **55**, 374 (1939).